JACS
JOURNAL OF THE AMERICAN CHEMICAL SOCIETY

Article

pubs.acs.org/JACS

Adenosine Triphosphate Hydrolysis Mechanism in Kinesin Studied by Combined Quantum-Mechanical/Molecular-Mechanical Metadynamics Simulations

Matthew J. McGrath,*[,†] I.-F. Will Kuo,[‡] Shigehiko Hayashi,[§] and Shoji Takada*[,†]

[†]Department of Biophysics and [§]Department of Chemistry, Graduate School of Science, Kyoto University, Sakyo, Kyoto 606-8502, Japan

[‡]Physical and Life Sciences Directorate, Lawrence Livermore National Laboratory, Livermore, California 94550, United States

Supporting Information

ABSTRACT: Kinesin is a molecular motor that hydrolyzes adenosine triphosphate (ATP) and moves along microtubules against load. While motility and atomic structures have been well-characterized for various members of the kinesin family, not much is known about ATP hydrolysis inside the active site. Here, we study ATP hydrolysis mechanisms in the kinesin-5 protein Eg5 by using combined quantum mechanics/molecular mechanics metadynamics simulations. Approximately 200 atoms at the catalytic site are treated by a dispersion-corrected density functional and, in total, 13 metadynamics simulations are performed with their cumulative time reaching ∼0.7 ns. Using the converged runs, we compute free energy surfaces and obtain a few hydrolysis pathways. The pathway with the lowest free energy barrier involves a two-water chain and is initiated by the $P_\gamma-O_\beta$ dissociation concerted with approach of the lytic water to $P_\gamma O_3^-$. This immediately induces a proton transfer from the lytic water to another water, which then gives a proton to the conserved Glu270. Later, the proton is transferred back from Glu270 to HPO_4^{2-} via another hydrogen-bonded chain. We find that the reaction is favorable when the salt bridge between Glu270 in switch II and Arg234 in switch I is transiently broken, which facilitates the ability of Glu270 to accept a proton. When ATP is placed in the ADP-bound conformation of Eg5, the ATP-Mg moiety is surrounded by many water molecules and Thr107 blocks the water chain, which together make the hydrolysis reaction less favorable. The observed two-water chain mechanisms are rather similar to those suggested in two other motors, myosin and F_1-ATPase, raising the possibility of a common mechanism.

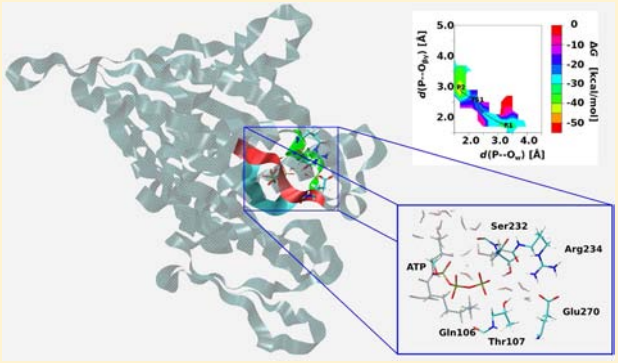

INTRODUCTION

The kinesin family of enzymes are molecular motors that use adenosine triphosphate (ATP) hydrolysis to proceed along microtubules, by which they participate in various essential cellular processes such as vesicle transport and chromosome segregation in mitosis.[1] Due to their importance, intensive studies have been performed on them for many years, resulting in motility and force generation characterization by single-molecule assays and other methods.[2,3] X-ray crystallography and cryo-electron microscopy have revealed structures with various bound nucleotides or their analogues, elucidating nucleotide-dependent conformational changes,[4] while mutagenesis and biochemical assays have implicated many residues in kinesin and tubulin as being essential for efficient function.[5] In contrast to these characteristics, much less is known for the molecular mechanism of ATP hydrolysis, primarily because of the lack of experimental methods that directly observe chemical reactions in proteins. Thus, theoretical studies of the ATP hydrolysis mechanism are highly desired, and yet no quantum chemical study has so far been reported for kinesin. Here we report, to our knowledge, the first quantum-chemical study on ATP hydrolysis mechanisms in kinesin.

Previous studies on ATP hydrolysis in proteins have suggested three key mechanistic issues. One is the idea of "associative" versus "dissociative" mechanisms. In an associative mechanism, the attacking nucleophile forms a bond with the terminal phosphorus before the ATP bond breaks. In a strictly dissociative mechanism, ATP bond cleavage precedes nucleophilic attack. The difference between these mechanisms is difficult to distinguish from experiments.[6] Theoretical studies of nucleoside triphosphate (NTP) hydrolysis and phosphoryl transfer in various proteins have suggested both associative and dissociative mechanisms, though most of the time the mechanism is concerted and simply leans toward one path or the other.

The second issue concerns the final acceptor of the proton removed from the lytic water molecule. Following the

Received: February 12, 2013
Published: May 23, 2013

   dx.doi.org/10.1021/ja401540g | J. Am. Chem. Soc. 2013, 135, 8908−8919

pioneering study on hydrolysis of triphosphate in an NTPase protein simulation,[7] theoretical studies of various NTPases have suggested that the inorganic phosphate generated by the hydrolysis reaction is the final proton acceptor.[8−13] On the other hand, theoretical studies on ATP hydrolysis in myosin[14,15] suggested that a proximal carboxylate accepts the proton in the product formation. Proton abstraction by a proximal carboxylate was also observed in F_1-ATPase,[13] although the proton acceptance is only transient and thus the carboxylate is characterized as a catalyzer rather than the group where the abstracted proton settles.

The last key issue for ATP hydrolysis mechanisms in molecular motors, that is, kinesin, myosin, and F_1-ATPase, is the presence of a water chain proton-shuttle mechanism. It should be noted that this issue also includes the number of water molecules involved in the reaction (commonly referred to as 1W versus 2W, as in the recent review of Prasad et al.).[16] The lytic water molecule that attacks the γ-phosphate of ATP is hydrogen-bonded to another water molecule. The latter plays a direct role in the removal of a proton from the lytic water molecule, acting as the proton acceptor or a mediator of proton translocation for formation of the formal nucleophile, OH^-. An initial study of a GTPase[7] explored the 1W mechanism as the logical first step, while subsequent computational and experimental studies for F_1-ATPase,[11,12] myosin,[8,13−15,17] and a G-protein[14] implicated a second water molecule playing a crucial role in the reaction. It has also been hypothesized that mediation of the proton translocation is fulfilled by hydroxyl groups of side chains of serine in the binding pockets of motor proteins.[9,18] It should be noted that water-chain mediated reactions are not specific to triphosphate hydrolysis, having also been seen or proposed in cytochrome P450cam,[19] carbonic anhydrase,[20,21] ethanol oxidation in supercritical water,[22] sulfur oxide hydration,[23] and proton translocation by water chains in cytochrome *c* oxidase,[24] gramicidin,[25] carbonic anhydrase,[26] and aquaporin.[27]

Experimentally, a recent crystal structure for Eg5, a member of the kinesin superfamily, directly resolved a two-water chain next to an ATP analogue, suggesting a similar role of the second water molecule.[28] Participation of mediating water molecules in the proton translocation was also suggested by a time-resolved Fourier transformed infrared spectroscopy (FTIR) study.[29] The authors of the FTIR study interpreted a continuum band observed upon the binding of the substrate as formation of a hydronium water cluster in the proton translocation, although the measurement is not able to capture a proton translocation at the transition state, which forms only transiently.

Motivated by these works on Eg5, we choose it as a target for quantum-chemical studies of ATP hydrolysis in kinesin. Eg5, a member of the kinesin-5 family, is known to function in mitosis during metaphase and anaphase.[30−34] The protein forms a homotetramer that has been shown to cross-link microtubules, with each dimeric head making short processive runs toward the plus end.[30,35] For Eg5, two crystal structures are available. The one that shows a two-water chain was crystallized in the presence of adenylyl imidodiphosphate (AMPPNP), a non-hydrolyzable ATP analogue (hereafter denoted as the ATP structure),[28] while another was crystallized in the presence of adenosine diphosphate, ADP (denoted as the ADP structure).[36] These Eg5 structures share overall architectural and major structural characteristics with other kinesin members, such as the switch I (shown in green in the top panel of Figure 1), switch II (red), and P-loop (blue) motifs.[28] Arg234 in switch I and Glu270 in switch II form an important salt bridge

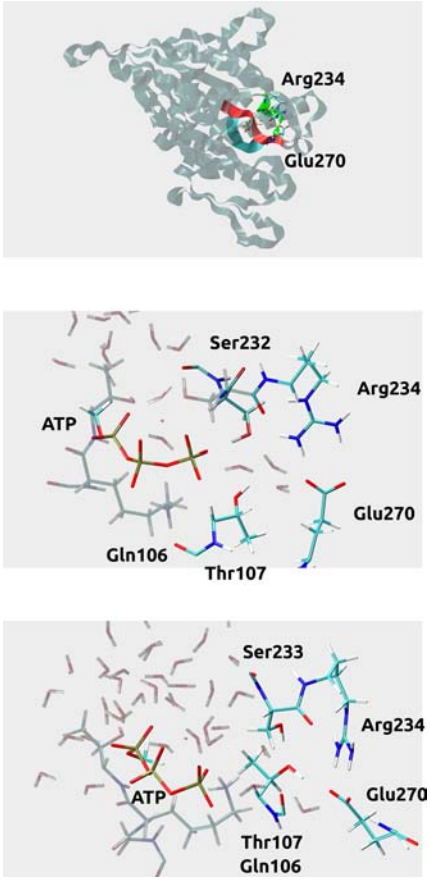

Figure 1. (Top) Picture of the Eg5 protein, along with representative snapshots of the active sites starting from the crystal structures of (middle) Parke et al.[28] and (bottom) Turner et al.[36] In the top structure, the P-loop, switch I, and switch II are depicted by blue, green, and red ribbons, respectively. In the middle and bottom structures, only the backbone carbonyl of the highlighted group is part of Gln106. In addition, all water molecules within 8 Å of the Mg ion are shown but not all protein residues, in order to enhance clarity.

for both structures. Mutations affecting this salt bridge are known to have significant impacts on structure and ATP catalysis in Eg5 as well as other motors.[35,37] Between these two structures, two important differences near the active site can be readily seen (bottom panels of Figure 1). First, in the ATP structure, the terminal phosphate of AMPPNP can interact with Glu270 of the salt bridge through a chain of two water molecules as mentioned above. In contrast, the ADP structure shows that the path is blocked by Thr107, although perhaps its hydroxyl group can play an analogous role to the second water. The second difference is the large number of water molecules found near the nucleotide in the ADP structure. The additional water molecules may create a more solutionlike environment around the Mg^{2+} ion, reducing the catalytic activity of the protein in this configuration.

In this paper, we explore ATP hydrolysis mechanisms in kinesin by using combined quantum mechanical/molecular mechanical (QM/MM)[38,39] metadynamics[40] simulations. Most previous QM/MM studies on molecular motors rely on searching the minimum energy path that connects the reactant and the product, with or without simple entropic corrections.

dx.doi.org/10.1021/ja401540g | J. Am. Chem. Soc. 2013, 135, 8908−8919

Use of metadynamics here enables us to incorporate thermally activated motions and to estimate free energy surfaces, although the sampling time is unavoidably limited. To our knowledge, a metadynamics QM/MM study for ATP hydrolysis has never been previously reported for molecular motors. One study has looked at hydrolysis in a protein,[41] however, and a very recent study examined phosphate hydrolysis in solution.[42] Extensive metadynamics simulations for reaction path searching and characterization based on free energy surfaces have been used for the first time in the present study to reveal key mechanisms of the catalytic hydrolysis of ATP in kinesin.

The paper is organized as follows. The next section discusses the setup of the QM/MM system and details of the metadynamics simulations. On the basis of the ATP and ADP structures of Eg5, we treat ∼200 atoms of the QM region by a dispersion-corrected density functional and conducted, in total, 13 different QM/MM metadynamics simulations, of which the cumulative sampling time reaches about 0.7 ns. Under Results, we obtain free energy surfaces and describe a few observed ATP hydrolysis pathways using the converged metadynamics runs. Then, under Discussion, we address how the ATP hydrolysis mechanism differs among the pathways and between ATP and ADP structures. We also briefly compare ATP hydrolysis mechanisms across different molecular motors.

SIMULATION DETAILS

Classical Molecular Dynamics. We first performed classical molecular dynamics (MD) simulations of Eg5 using a molecular mechanics (MM) based force field, of which the purpose is 2-fold: (1) to generate configurations that may be able to readily undergo ATP hydrolysis in the QM/MM metadynamics runs and (2) to determine the robustness of the initial crystal structure.

The Eg5 crystal structures of Parke et al.[28] (PDB code 3HQD) and Turner et al.[36] (PDB code 1II6) were used as starting points for all subsequent manipulations. We shall refer to these as the ATP and ADP structures, respectively, since 3HQD was crystallized with a nonhydrolyzable ATP analogue (AMPPNP) while 1II6 was crystallized with ADP. It should be noted here that Eg5, like all members of the kinesin superfamily, hydrolyzes ATP in vivo while bound to microtubules. The lack of available crystallographic data prevents us from examining such a state here. More importantly, it is known that kinesins do hydrolyze ATP even without binding to a microtubule, albeit with a reduced rate constant. As Eg5 in the presence of AMPPNP crystallizes as a dimer, one Eg5 molecule (including the associated Mg, AMPPNP, and waters) was removed. The AMPPNP molecule in the active site was changed into ATP, and hydrogens were added by use of the psfgen program provided with NAMD 2.8, which also charges acidic and basic residues. A similar procedure was carried out for the ADP structure; in addition, the ADP is replaced by ATP. As some residues are missing from this structure, they were modeled by the MODELER program.[43] Eg5 contains seven histidine residues. As two of the residues (His141 and His205) are in close proximity to acidic groups, the rest of the steps described in this section were performed with two separate configurations: one with seven neutral histidine residues, and one where His141 and His205 are protonated. The closest histidine to the active site is His236, which lies about 9 Å away from the γ-phosphate of ATP and not close to any acidic groups; it is therefore unlikely that the protonation states of the histidines will play a major role in the metadynamics calculations. Regardless, this issue is examined in more detail below.

The above structures were solvated by use of the solvate plugin of VMD,[44] including about 15 Å of extra space on each side of the protein to ensure decoupling of periodic images. This resulted in a box measuring 85 × 85 × 105 Å and containing around 73 000 atoms. Sodium atoms were added to neutralize the charge and were placed to minimize their effect on the protein. We used the CHARMM27 force field to describe the protein and ligands,[45,46] while water was described by the TIP3P model.[47] Since ATP coordinated to Mg^{2+} under physiological conditions is almost certainly fully deprotonated,[48] we use ATP^{4-} in all initial structures. All classical MD simulations were carried out with the GROMACS package.[49] The three configurations (ATP with the protonated and unprotonated His141 and His205, and ADP with only the unprotonated residues) were energy-minimized for 5000 steps, prior to 1 ns of equilibration in the canonical ensemble. SETTLE[50] and P-LINCS[51] were used to keep all the bond lengths constant, and the Berendsen thermostat[52] kept the simulation temperature at 300 K. We used a nonbonded cutoff of 12.0 Å, along with a time step of 1 fs. The smooth particle mesh Ewald technique[53] was used to compute the long-range electrostatic interactions.

With these setups, we performed a series of 40 ns classical MD runs using slightly different simulation parameters and starting structures, including configurations with both protonated and unprotonated histidine residues described above, ATP and ADP structures, and the canonical and isobaric−isothermal ensembles (given the size of the system, the volume fluctuations are expected to be relatively small). No significant difference in the root-mean-square deviation (RMSD) of the heavy protein atoms was observed after the trajectories, indicating only minor influences of the simulation parameters and the starting configurations. Small RMSDs (2.0−3.0 Å) after equilibration indicate that the initial crystal structures are relatively stable. We identified several likely reaction structures in the trajectories of the ATP and ADP structures, respectively (see Results).

Quantum Mechanics/Molecular Mechanics Calculations. The MM region was described with the CHARMM27 force field, including the additional terms for ATP. A smooth particle mesh Ewald sum[53] with a grid of 88 × 88 × 108, a fourth-order spline, and a nonbonded cutoff of 12.0 Å were used for calculation of the electrostatic energies. The QM region was designed to include the phosphate of ATP, the full coordination shell of the Mg^{2+} ion, and any water molecules and protein residues that appeared as though they could participate in the reaction. The QM regions were kept identical between all simulations starting from the same crystal structure (except for the water molecules, as these drifted significantly during the course of the MM MD simulations). In the ATP structure, this included residues Thr107, Gly108, Gly110, Lys111, Thr112, Thr226, Asn229, Ser232, Ser233, Arg234, Ala267, and Glu270. In the ADP structure, this included Thr107, Gly110, Lys111, Thr112, Ser233, Arg234, Ala267, Gly268, and Glu270. The difference in the residues included in the simulation for the two structures is because the ADP structure is significantly more "open", resulting in a displacement of some residues by water molecules. The total number of QM atoms in both cases is around 200 but not identical, due to additional water molecules being included in the QM region for the ADP structure. The boundaries between the QM and MM regions were set to be at the (O)C−C(N) backbone bonds for the proteins. We used a link-atom approach with hydrogen atoms to close the valence of the QM region. For the interaction between the QM and MM region, we have chosen to use the Gaussian expansion of the QM/MM electrostatic potential (GEEP) method[54] to smear out the MM charges closest to the QM region with seven Gaussian functions. It should be noted that the charge redistribution scheme becomes less of an issue with increasing system size,[55] and our large QM system here should give reasonable results.

The quantum mechanical/molecular mechanical (QM/MM) calculations were carried out with CP2K, a freely available simulation suite.[56] The QUICKSTEP routines compute the energy of a system by use of Kohn−Sham density functional theory,[57] expanding the molecular orbitals in a localized Gaussian basis set and the electronic density as a set of plane waves; this allows for efficient calculation of the system energy.[58] We chose the exchange−correlation functional of Becke−Lee−Yang−Parr (BLYP)[59,60] and added the most recent dispersion correction by Grimme et al.[61] BLYP with empirical dispersion corrections has been shown to perform better than other pure functionals for biological molecules.[62] Functionals with exact exchange are cost-prohibitive for the present purpose. While BLYP tends to underestimate reaction barriers, very few data exist for the specific reaction of ATP hydrolysis. However, a recent study has

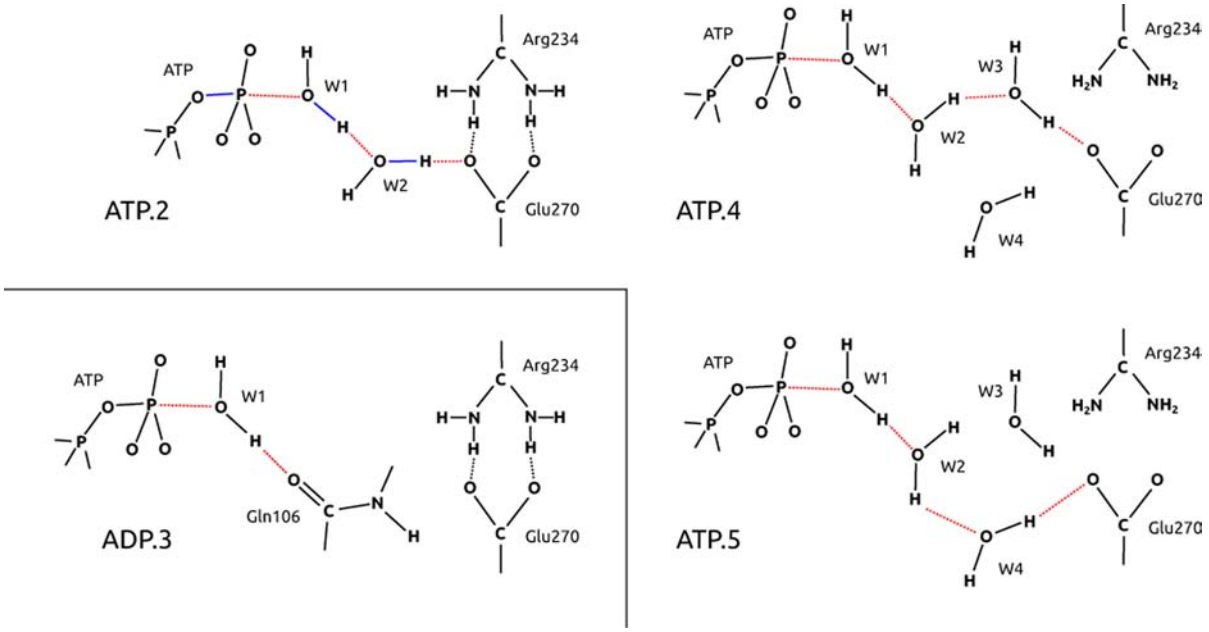

Figure 2. Collective variables of the principal runs in this work. Red and blue lines indicate that the distances are added or subtracted from the colvar, respectively. Solid and dashed lines indicate bonds formed in the initial (reactant) structure and the final (product) structure, respectively. Numbers indicate the legend used in Figures 3 and 4.

explored methyl triphosphate hydrolysis in solution, making use of BLYP and metadynamics.[42] The authors report an activation barrier height within a few kilocalories per mole of the experimental estimate. For the potential of mean force computed for ATP in solution with BLYP and a dispersion correction, the activation barrier was found to be higher.[63] Additional discussion on the density functionals can be found in the Supporting Information. We used a triple-ζ split-valence basis set with two polarization functions (TZV2P) and a plane-wave cutoff of 320 Ry for the QM region.

Metadynamics. While geometry optimizations on the potential energy surface grant insight into stable structures and possible reaction paths, they do not take into consideration configurational entropy, which may cause significant errors for enzymatic reactions.[64] Therefore, we used the metadynamics technique (also known as the "hills" method) pioneered by Laio and Parrinello[40] to explore the free energy surface of the ATP hydrolysis reaction in Eg5. There are several excellent reviews available covering both the method and its various extensions,[65−67] so we will not cover it in detail here. Suffice it to say, the method operates by identifying a small number (typically one or two) of collective variables that describe the free energy barrier of interest and evolve the system in an extended Lagrangian formulation, adding small repulsive Gaussian functions to discourage the system from revisiting regions of space it has already seen. In the long-time limit, it can be shown that the sum of these repulsive potentials is related to the underlying free energy surface of the system.[68] We also clarify here that metadynamics is not the only approach currently capable of generating free-energy surfaces in enzymes. The empirical valence bond (EVB) method has been used for many years for this purpose (see Kamerlin and Warshel[69] for a recent review summarizing the method and its applications, including a study in 2003 on F1-ATPase[70]), and the recently developed paradynamics method[71] (PD) is also very promising.

It should be noted here that due to the complexity of the free energy surface of this reaction and all the possible degrees of freedom, the purpose of this study is to compare the reaction free energies for a series of different reaction paths and initial structures. This is not the philosophy behind the metadynamics method, whose strength lies in the ability to explore reactions without an a priori guess of the reaction path.[72] It is possible that other methods may be better suited to this particular task,[71] but practical considerations have led us to use metadynamics.

In order to run the metadynamics simulations with QM/MM, we had to run short QM/MM MD simulations in the canonical ensemble to equilibrate the structures with mixed interaction energies. This involved attaching a Nose−Hoover chain of length three to every molecule in the system and running molecular dynamics until the temperature stabilized (approximately 3−4 ps). A simulation time step of 0.5 fs was used, and the internal geometry of all water molecules in the MM region was fixed with a 3 × 3 constraint. The metadynamics simulations were started immediately afterward. Repulsive Gaussian potentials were placed every 20 fs. Initially, their height was 0.003 hartree and their width was 10% that of the associated collective variable. Once a simulation visited the product state and returned to the reactant, the height of every hill previously deposited was scaled by 0.90 and the simulation was restarted, using new hills with a height of 0.001 hartree in an attempt to smooth out the free energy surface and improve sampling (these runs are designated with the extension SCALED). The original height, width, and deposition frequency follow the guidelines suggested by Laio et al.[73] and those used in previous studies.

RESULTS

Initial Structures and Collective Variables of Hydrolysis Reaction. We were able to identify three likely reaction structures from the ATP structure of the classical MD trajectory (see Simulation Details), which involve the experimentally proposed two-water chain and two three-water chains, one with a broken Arg234−Glu270 salt bridge and the other with the bridge still partially intact. Four different structures were found from the ADP structure. Details of the configurations are given under Metadynamics. This gave us a total of seven configurations to explore in depth with quantum mechanics/molecular mechanics (QM/MM) simulations.[38] These seven configurations (three from the ATP structure and four from the ADP structure) were selected because they appeared to be ready to undergo ATP hydrolysis due to the position of the ATP, surrounding residues, and nearby water molecules. This is necessary given the short simulation length accessible with QM/MM simulations. One of the configurations was selected because it closely resembled the ATP structure where two

dx.doi.org/10.1021/ja401540g | J. Am. Chem. Soc. 2013, 135, 8908−8919

waters form a bridge between Glu270 and the γ-phosphate of ATP. Some of the reaction paths (for example, using a carbonyl group as a proton relay) may seem unusual. We selected pathways that seemed possible in the classical MD simulations in an attempt to explore a variety of options, under the assumption that any path which was truly unfavorable would either not complete the metadynamics run or generate a high barrier. Multiple choices of collective variables (see below) were attempted for several of the configurations, bringing the total number of runs to 13 (see details below and in Table S1 in the Supporting Information). For notation purposes, runs that start from the structure crystallized with an ATP analogue are labeled ATP.*N*, while those from the structure crystallized with ADP are labeled ADP.*N*.

The single most important parameter choice in a metadynamics simulation is the choice of collective variable (colvar), as a poor choice of colvar can lead to drastic overestimation of the barrier height.[66] Ideally, the colvars should clearly distinguish between the important states, describe all the important slow events, and be few in number. This last criterion is the most difficult for our current system, due to the possibility of multiple residues being involved in addition to several waters and the ATP. It is for this reason that we limited ourselves to two colvars: one that describes the reaction path and one that serves as a "constraint" on the reaction path. Running a completely open-ended metadynamics simulation for this system is cost-prohibitive, and therefore we chose to focus on several possible reaction paths and compare the relative barrier heights. The four most important colvars are shown in Figure 2, while the other nine are given in the Supporting Information. Significant differences between the initial configurations and collective variables are summarized in Table S1 in the Supporting Information.

Metadynamics Runs. With these setups, we performed 13 independent metadynamics runs (Table S1 in Supporting Information). One crucial decision that needs to be made during a metadynamics simulation is when to terminate the run. Raiteri et al.[74] reiterated a previous suggestion by the same group that metadynamics simulations be stopped immediately after a recrossing event through the same reactive pathway in the case of two basins. As the collective variables (colvars) used in these runs contain multiple distances, it is not sufficient to rely on simply the value of the colvar to determine the "reactant" and "product" states. Instead, we used this value as a guide to visually confirm when the systems were in the reactant (i.e., the chemical bonds are the same as the initial structure) and product (the chemical reactions selected by the colvars had all occurred) states. We have indicated which simulations contain recrossing events in Table S2 in Supporting Information, and we used this as a basis for rescaling certain runs. In total, four out of 13 runs were successful (ATP.2, ATP.4, ATP.5, and ADP.3), in addition to one of the rescaled runs (ADP.3.SCALED).

Metadynamics "Trajectories". The metadynamics method uses coarse-grained dynamics of selected variables to bias the dynamics of the system and circumvent free energy barriers.[66] This means that the dynamics seen in these trajectories are not the true dynamics of the system. However, examining molecular motion observed in the trajectories often provides us with insights into mechanistic aspects of the reactions. In an effort to elucidate the actual reactions that took place during the simulations, we have plotted various geometric parameters of the system in the reactions of ATP.5 and ADP.3 as a function of simulation time in Figures 3 and 4, respectively, including snapshots of the system with arrows depicting the reactions at various points. We focus on ATP.5 and ADP.3 because the former gives the lowest activation barrier (see below) and the latter is the only successful run from the ADP structure. The corresponding plots for ATP.2 and ATP.4 are shown as Figures S10 and S11 in the Supporting Information. For clarity, all of the data points in Figures 3 and 4 have been averaged over the surrounding 50 frames to reduce the noise of short-term fluctuations.

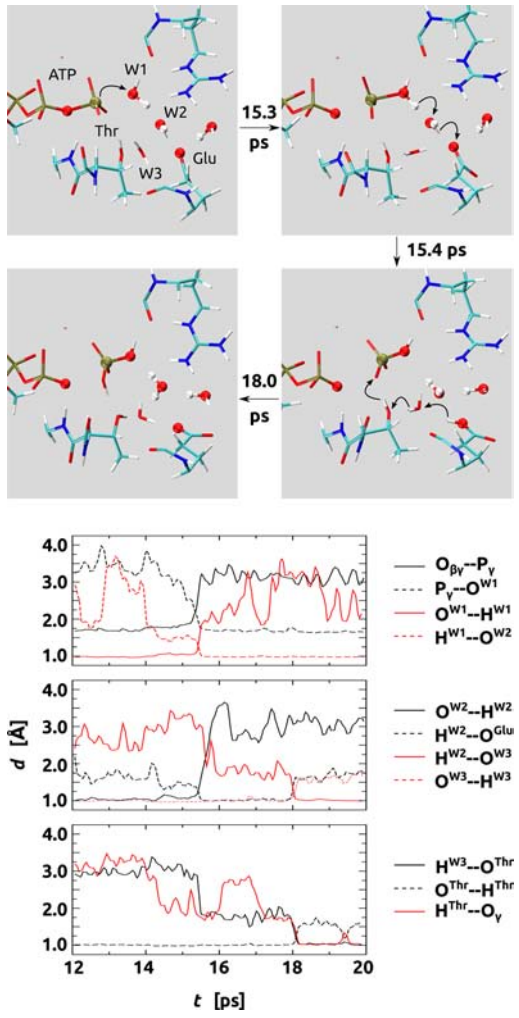

Figure 3. Major chemical reactions that occur in ATP.5. (Top panels) Black arrows indicate reactions, with the approximate time indicated between panels. Colvar atoms are indicated with spheres. (Bottom panels) Values of various distances as a function of simulation time, beginning from the commencement of hill placement after the initial MD run. The midpoints of individual reactions happen at 15.3 (black) and 15.4 (red) ps, 15.4 (black) and 18.0 (red) ps, and 18.1 (black) ps for the three bottom panels, respectively.

As seen in Figure 3, the reaction process of ATP.5 starts with formation of a metaphosphate by dissociation of P−$O_{\beta\gamma}$ bond and simultaneous coordination of a lone pair of the lytic water molecule (W1) to a vacant orbital of the metaphosphate at 15.3 ps. Immediately after the event, a proton of the lytic water molecule transfers to the carboxyl group of Glu270 in a concerted way via a relaying water molecule (W2) at 15.4 ps. The proton transfer accompanies formation of an inorganic

dx.doi.org/10.1021/ja401540g | J. Am. Chem. Soc. 2013, 135, 8908−8919

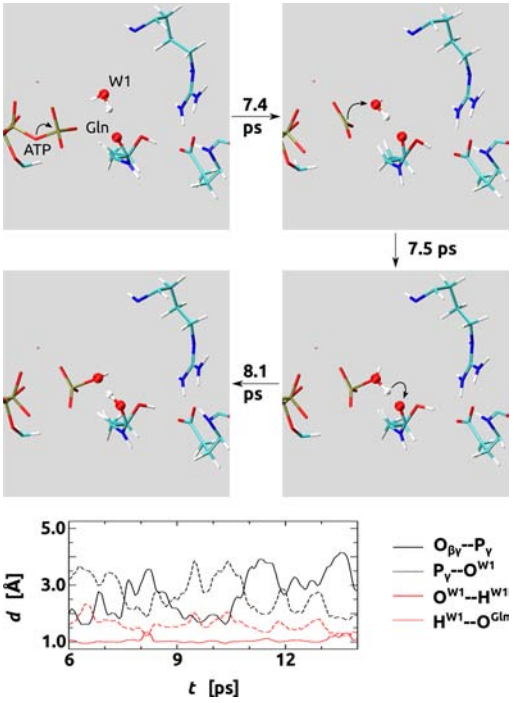

Figure 4. Major chemical reactions that occur in ADP.3. (Top panels) Black arrows indicate reactions, with the approximate time indicated between panels. Colvar atoms are indicated with spheres. (Bottom panel) Values of various distances as a function of simulation time, beginning from the commencement of hill placement after the initial MD run. Midpoints of the first chemical reaction occur at 7.5 and 8.1 ps for the black and red curves, respectively.

phosphate, HPO_4^{2-}. Then the reaction is completed by concerted proton transfers from the carboxyl group to the inorganic phosphate through a water molecule (W3) and the hydroxyl group of Thr107 at 18.0 ps. Consequently, ADP and $H_2PO_4^-$ are formed in the product state. An animation of this reaction is included in the Supporting Information.

The reaction process of ATP.2 with an intact Arg234–Glu270 salt bridge resembles that of ATP.5, as shown in Figure S10 in the Supporting Information. The only difference is that the same water molecule (W2) relays both the first proton from the lytic water molecule (W1) to Glu270 and the second proton from Glu270 to HPO_4^{2-}. However, the reaction process of ATP.4 terminates at the protonation of Glu270 by a proton transfer from the lytic water molecule via the hydroxyl group of Ser233 and a water molecule (W2) (Figure S11 in the Supporting Information). Consequently, the generated inorganic phosphate stays singly protonated, that is, HPO_4^{2-}.

As seen in Figure 4, the first event of the reaction of ADP.3 in the ADP structure is the same as that in ATP.5: formation of a metaphosphate and coordination of the lytic water molecule to it at 7.4 ps. However, a subsequent proton transfer at 8.1 ps occurs to the oxygen of the backbone carbonyl group of Gln106, driven by the colvar definition. The proton is further transferred to the inorganic phosphate and the final product state of ADP and $H_2PO_4^-$ is formed (not shown in Figure 4). This reaction is also animated in the Supporting Information.

We applied the reweighting scheme of Bonomi et al.[75] to the simulations for all the successful runs, which enabled us to calculate free energy surfaces for any reaction coordinate. In order to estimate the error in the free energy surface by the reweighting scheme, we compared the free energy profiles of run ATP.2 evaluated by the reweighting scheme with that of the negative of the cumulative biasing potential (see Figure S7 in the Supporting Information). The mean unsigned error between the points is 3 kcal/mol, which we will take to be our free energy error for the rest of this paper. It should be stressed here that this estimate is only for the sampling error, that is, the error due to the finite simulation length. There will also be an additional error due to the various assumptions made in the calculation of the interaction energies that we cannot reliably calculate.

The simulation community has long understood the need to perform reliable simulations. The work of Frushicheva et al.,[76] for example, maintains that the most reliable results are obtained by a method that can reproduce experimentally observed catalytic effects and pK_as. While we agree with the spirit of this work, the expense of QM/MM metadynamics simulations clearly precludes validation by the method in that work, at least in a single paper. This is made worse by the many available options for the QM portion of QM/MM metadynamics, each of which have their own strengths and weaknesses. The validation of QM/MM metadynamics must therefore be a community project. The present work consists of part of that validation by examining two different Eg5 structures, one of which is expected to be more favorable to catalysis than the other. As our finding agrees with prior intuition with regard to the relative barrier heights in these structures, this gives one more confidence in the method and density functional used.

Applying the reweighting scheme, we generated various free energy surfaces along identical sets of reaction coordinates for all four converged runs, which makes it possible to compare free energy surfaces for the runs that used different colvars. After trying many coordinates, we found a particular choice of the pair of reaction coordinates useful: the distance $d(P\cdots O_{\beta\gamma})$ between the γ-phosphate on ATP and the link oxygen atom $O_{\beta\gamma}$ between the β- and γ-phosphate, as well as the distance $d(P\cdots O_W)$ between the γ-phosphate and the oxygen atom O_W of the attacking water molecule. This set of reaction coordinates is important, as it is the distinguishing factor between the associative and dissociative reaction mechanisms.

The free energy surfaces for all four successful metadynamics simulations are shown in Figure 5. All of the ATP.*N* runs show two distinct wells separated by free energy barriers at transition states. The ADP.3 run, while showing a very deep well for the reactant state, has a much shallower well in the product state, suggesting that this ADP structure is not as favorable for the inorganic phosphate and ADP molecule.

Figure 5 indicates that all of the transition states involve broken ADP–P_i bonds. It appears that the ATP terminal phosphate bond begins to break upon the approach of water to around 3 Å, after which the breaking of the ATP bond is closely correlated with the distance between the phosphorus and attacking water molecule. This suggests that there is a concerted mechanism at work, in particular in runs ATP.4 and ATP.5. In run ADP.3, the breaking of the phosphate bond appears to occur earlier than the water molecule's approach, almost completing before the water moves the final angstrom to form the inorganic phosphate. This suggests a dissociative mechanism in run ADP.3. These results taken together indicate that dissociative and concerted reaction pathways are the most relevant to the Eg5 system, although it must be noted that the dissociative mechanism is only seen in a pathway that is much more unfavorable and therefore would not occur in the real system.

dx.doi.org/10.1021/ja401540g | J. Am. Chem. Soc. 2013, 135, 8908–8919

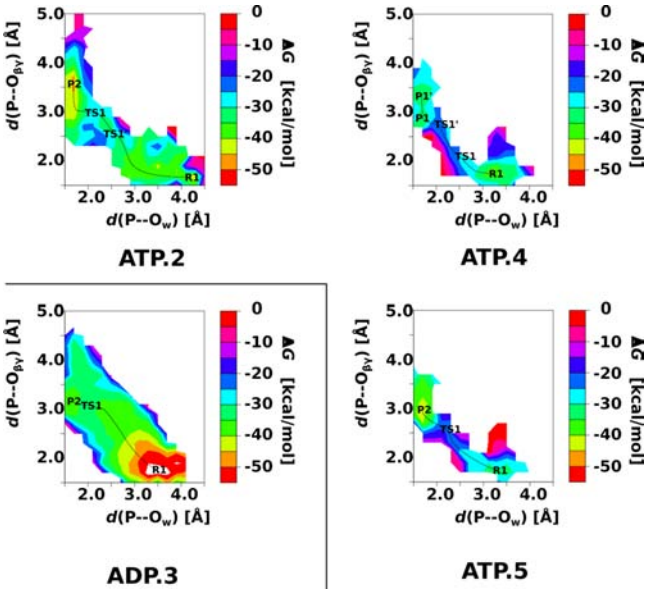

Figure 5. Free energy as a function of both the distance between the terminal phosphorus and the attacking water as well as the phosphorus and the $\beta-\gamma$-link oxygen. Reactant, transition state, and product regions are indicated with R, TS, and P, respectively. A prime indicates a structure of lesser importance, i.e., a more stable transition state or less stable product state.

It should be noted that since the two coordinates of the free energy surfaces in Figure 5 are not sufficient to represent the complex paths of the entire reaction processes described above, some of the free energy wells of the reactant and product states contain minor conformations. Schematic views of the conformations in the chemical states of ATP5, ADP3, ATP2, and ATP4 are summarized in Figures 6 and 7 and Figures S8 and S9 (Supporting Information), respectively. For example, the P2 well of ATP.5 includes both the product state and the intermediate state where Glu270 accepts a proton. As described above, since such intermediate states live only transiently, their contributions to the reaction free energies are minor.

The free energies of all the marked states in Figure 5 are shown in Figure 8, using the free energy difference relative to the reactant state. Within the uncertainty of our calculations, the reaction barriers for runs ATP.4 and ATP.5 are approximately the same, while ATP.2 is slightly less favorable. ADP.3, on the other hand, is significantly less favorable, displaying a free energy barrier almost twice as high as that of ATP.5. The product state free energies are even more revealing. ATP.5 finds a product state that is quite stable relative to the reactant state, while ATP.2 and ATP.4 show products that are approximately as stable as the reactants. Again, ADP.3 shows the least stable product, almost 20 kcal/mol higher in energy than the reactant state and only slightly more stable than the transition state. It should be mentioned here that this analysis assumes the free energies for all reactant states are equal. This is clearly true for ATP.4 and ATP.5 (which start from the same structure). However, one can also assume that the initial structures for ATP.4 and ATP.5 (in particular, the broken salt bridge) are not too much more unstable than the others with an intact salt bridge as we observed the breakage in the classical MD simulation on a time scale of tens of nanoseconds. The salt bridge probably would have re-formed before the end of the classical MD run had this conformation been very unfavorable (which it did not). A similar observation can be made for the

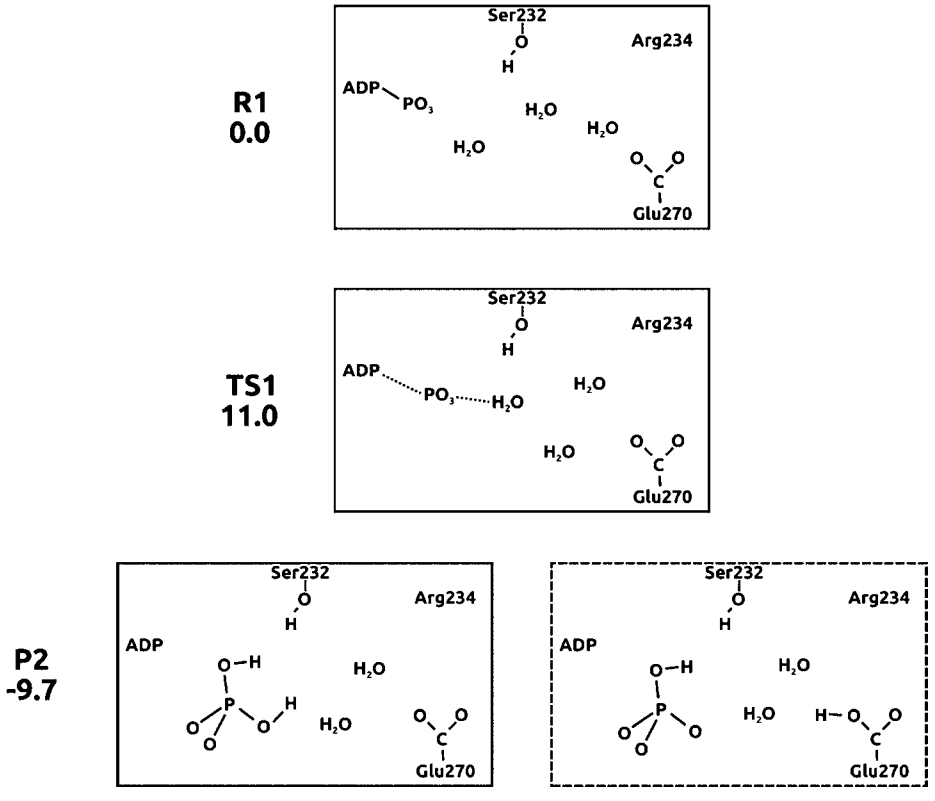

Figure 6. Schematic representations of the reactant, product, and transition-state structures marked in Figure 5 for run ATP.5. A solid box indicates the most stable structure at each point.

dx.doi.org/10.1021/ja401540g | J. Am. Chem. Soc. 2013, 135, 8908−8919

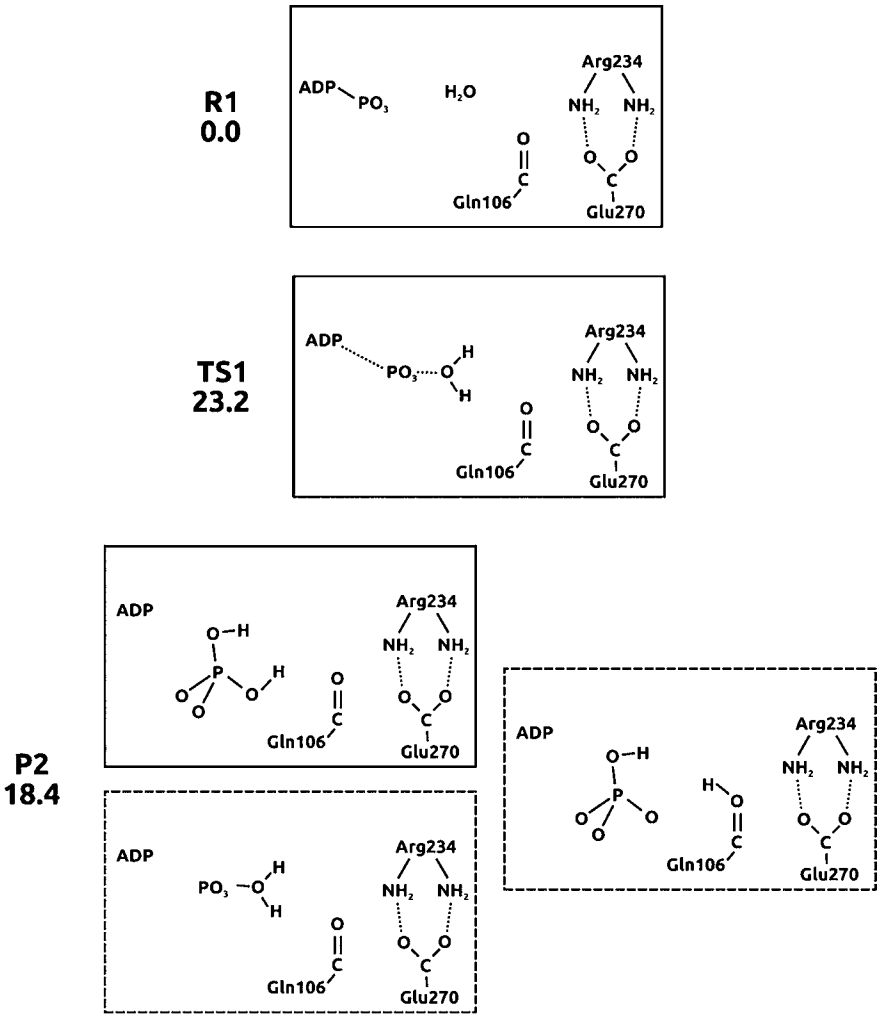

Figure 7. Schematic representations of the reactant, product, and transition-state structures marked in Figure 5 for run ADP.3. A solid box indicates the most stable structure at each point.

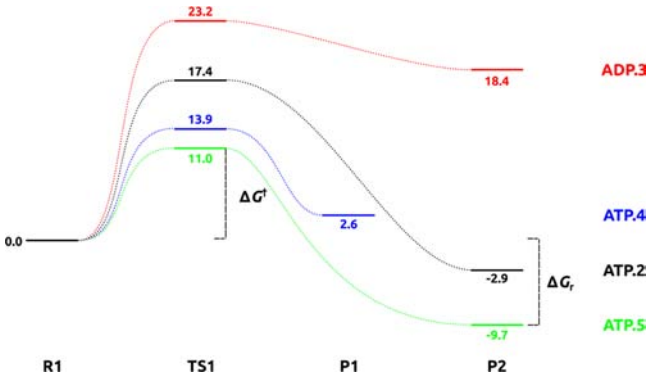

Figure 8. Comparison of free energies calculated for all the important states indicated in Figure 5.

presence of the third water molecule in the active site, which is not seen in the X-ray structure of Parke et al.[28] and which seems to be related to the state of the salt bridge (see Table S1 in the Supporting Information). Future extensive molecular mechanical MD simulations exploring the stability of the various states would be very beneficial, although they are outside the scope of the present work.

Experimentally, Cochran and Gilbert[77] and Cochran et al.[78] show that monomeric Eg5 in solution in the absence of microtubules catalyzes ATP at a rate of 1.14 s^{-1}. If we use the transition-state theory with the standard prefactor,[79] this corresponds to a barrier of 17.5 kcal/mol, which is above the lowest barrier height (11.0 kcal/mol for ATP.5) that we report in Figure 8. This difference could be due to the issue with pure GGA-corrected density functionals noted above, which are known to overstabilize the transition state in some reactions. Furthermore, the breakage of a salt bridge in the ATP.4 and ATP.5 initial conformations costs additional energy compared to the ATP structures with an intact salt bridge. In addition, the conversion of a measured enzymatic reaction rate to an activation free energy barrier has some inherent uncertainty. When those facts are taken into account, the computed free energy barrier is in reasonable agreement with the experimental evidence. Despite the quantitative discrepancy of the free energy barrier, the distinct differences in the free energy profile among the successful paths enable one to characterize clearly mechanistic features of the reaction as seen below.

DISCUSSION

Is ATP Hydrolysis Associative, Dissociative, or Concerted? In the present simulation, the first event of the hydrolysis reaction, which is also the rate-determining step, appears to include significant elongation of the P_γ−$O_{\beta\gamma}$ bond in concerted bond rearrangement at the γ-phosphate. This

dx.doi.org/10.1021/ja401540g | J. Am. Chem. Soc. 2013, 135, 8908−8919

observation contradicts an associative mechanism proposed by Jun and Kim[29] on the basis of a UV-photolyzed FTIR study of the caged Eg5 monomer in aqueous solution in the absence of microtubules, which, to our knowledge, is the only previous study on the reaction mechanism of ATP hydrolysis in Eg5 (although an examination of the QM/MM optimized structures of myosin and Eg5 led Nemukhin et al.[80] to conclude that a dissociative mechanism is favorable in Eg5). They observed a continuum IR band, which was interpreted as an organized water cluster solvating a proton and thus generating the nucleophile hydroxide ion as the counterpart. As the continuum IR band appeared just after the substrate binding and well prior to formation of the product inorganic phosphate, the experimental observation disfavors a dissociative mechanism where formation of the inorganic phosphate takes place before attack of the nucleophile.

In the present simulation, as described above, none of the reactant nor the transition states include a hydroxide ion forming and attacking the γ-phosphate. Although a hydroxide ion is a much stronger nucleophile than a water molecule and thus could facilitate bond rearrangement at the γ-phosphate, formation of a hydroxide ion by removing a proton from the lytic water molecule requires a large energy cost as is indicated by a very high pK_a of water, 15.7. Moreover, for the hydrolysis reaction, a negatively charged ion of hydroxide needs to be created in the vicinity of a negatively charged group of the γ-phosphate, which formally carries a charge of −2|e|. The large electrostatic destabilization together with the intrinsic high energy cost for splitting a water molecule, as was also found in a previous study for F_1-ATPase,[13] appears to prevent the energetically unfavorable formation of a hydroxide ion in the trajectories even when the colvars employed in the simulations included reaction coordinates capable of describing hydroxide ion formation.

On the other hand, the present trajectories show that removal of a proton from the lytic water molecule is strongly stabilized by concerted bond formation between the water molecule and the metaphosphate dissociated from ADP occurring almost simultaneously. The concerted profile therefore manifests a key catalytic mechanism of the reaction by avoiding explicit formation of an unstable hydroxide ion. Formation of the metaphosphate stimulating the proton removal is also suggested to be catalyzed by interaction of the β-phosphate in ADP with the P-loop (Walker A motif) of the protein. Such a chain activation of the γ-phosphate and the lytic water molecule is also found in catalysis of F_1-ATPase.[13]

The different views proposed by the FTIR study[29] and the present theoretical analysis would be reconciled by explicit assignment of the observed continuum IR band. It has not been determined precisely which groups in the protein are responsible for the continuum band. It is also noteworthy that a recent theoretical study has suggested that a continuum IR band can appear without explicit formation of a solvated proton.[81] Calculation of an IR spectrum will provide theoretical insight into role of the chemical phenomena underlying the continuum band in the hydrolysis reaction catalysis.

Proton Translocation in Hydrolysis. In all of the successful trajectories of ATP structures, a water molecule that resides between the lytic water molecule and Glu270 participates in relaying the proton transfer from the former to the latter upon P_γ−O_W bond formation. It should be noted that, as seen in Figure 3 and Figures S10 and S11 (Supporting Information), formation of a quasi-stable hydronium ion of the second water molecule with a discernible lifetime is not observed in the processes, indicating that the second water molecule serves as a mediator of the proton translocation rather than a proton acceptor. As described above, involvement of the second water molecule in the hydrolysis reaction has been suggested for various ATPase motor proteins such as F_1-ATPase and myosin as well as Eg5. Given the structural similarities between these motor proteins, it is plausible that these proteins share the mechanism of proton translocation by the second water molecule.

It is noteworthy that in run ATP.5, which gives the most energetically favorable reaction path, only one water molecule (W2) appears to participate in the relay of the proton from the lytic water molecule to Glu270 (Figure 3), despite the fact that the colvar of ATP.5 includes two water molecules (W2 and W4) situated between the proton donor and acceptor groups (Figure 2). Similarly, in the second proton transfer from Glu270 to the γ-phosphate, the proton proceeds through the hydroxyl group of Thr107, which is not included in the colvar. These observations that the proton translocation paths found are not entirely mandated by the colvar indicate that the metadynamics approach successfully allowed us to find energetically more stable paths than those assumed by the colvar, which would be a formidable task by a minimum potential energy path search for a flexible hydrogen-bond network system including many exchangeable hydrogen bonds.

In run ATP.4, a hydroxyl group of Ser232 intervening between the lytic water molecule and the second water molecule also participates in the proton relay. Since the activation free energy of ATP.4 is as low as that of ATP.5, the hydroxyl group is suggested to be capable of acting as a mediator of the proton translocation. In run ATP.4 for Eg5, however, a stable path in a process following the proton transfer to Glu207 was not found, thus disfavoring the reaction path represented by ATP.4 (see below). The use of serine in the reaction mechanism has been explored in detail for for myosin[82,83] and F_1-ATPase,[18] although those studies focused on transferring the proton directly to the inorganic phosphate. Our simulation that explored a direct route using a serine was unsuccessful (ADP.1). The simulation crossed to the product state very late in the trajectory (at 40.6 ps, it was the second slowest simulation; see Table S2 in the Supporting Information). This suggests that the barrier is higher than the others we observed, although without the recrossing back to the reactant state we do not feel sampling is sufficient to make concrete observations. From the MM trajectories used to generate the initial configurations for the QM/MM metadynamics, no other configuration had the serine in a likely position to assist in the reaction.

In the product formation after proton transfer to Glu270, the proton is further shuttled to the γ-phosphate in runs ATP.3 and ATP.5, although a pathway to this product was not described by those colvars (though we attempted several that included it). Consequently, the γ-phosphate is the final proton acceptor in those runs. On the other hand, in the case of ATP.4, further reactions after the proton transfer to Glu270 are not observed, and thus Glu270 is the final proton acceptor. Energetics of the different protonation states in the product states can be deduced from comparison between free energies of the product states of ATP.4 and ATP.5 shown in Figure 8; the initial structures of those runs are the same and thus free energies of the reactant states of those runs coincide. The large free energy difference between the product states (12.3 kcal/mol) suggests

that the γ-phosphate is the final proton acceptor, and Glu270 acts as a catalyst for proton translocation.

One very interesting question in systems involving proton translocation across multiple water molecules is that of the actual mechanism of proton transfer. As summarized by Kato et al.,[27] there are two theories suggested in the literature: one in which the reorientation of water molecules is of primary importance and the second in which the electrostatic barriers to the movement of the proton are more important. While this question is certainly important, the semiunconstrained dynamical nature of this study makes it impossible for us to address it. The water molecules are too flexible to permit significant orientation analysis, and the transition states are too transient to compute a free energy profile. Therefore we refer the interested reader to the review of Kato et al.[27] and references therein.

One-Water versus Two-Water Mechanisms. Prasad et al.[16] have recently summarized much of the current work on 1W versus 2W mechanisms in phosphate hydrolysis, pointing out some of the issues raised with various methods. Even though the implicit solvent calculations performed in that work are not perfect (pointed out by the authors themselves), an important conclusion is made. Metadynamics remains a powerful tool, but there is some danger in its misuse, as with any other tool. The major limitation in the present work is the lack of explicit consideration of a 1W mechanism where the attacking water transfers the proton directly to the phosphate. As noted above, one of the advantages of the metadynamics approach is its flexibility, and the fact that such a mechanism was not seen in one of the collective variables attempting a two-water chain to deposit a proton on the phosphate suggests that such a mechanism is unfavorable in our system. However, this is not conclusive proof, and future studies should consider the 1W mechanism explicitly.

Role of Protein Conformational Changes in Catalysis of Hydrolysis. The major difference between ATP.5 and ATP.2 is the broken Arg234−Glu270 salt bridge. This breakage appears to promote the reaction by raising the pK_a of Glu270, which makes it more ready to act as a proton relay. In addition, Arg234 in ATP.2 moves ∼2 Å away from the γ-phosphate near the beginning of the simulation. This reduces its ability to stabilize formation of the inorganic phosphate, which leads to the decreased stability of the product state relative to ATP.5.

The large free energy differences in the reactions between the ATP and ADP structures can be partially explained by the structures of the respective runs. As noted above, all of the ADP crystallographic structures are much more open than the ATP ones, resulting in more water near the active site (see Figure 1). This creates a more aqueouslike environment around the Mg^{2+} ion. As the function of these proteins is to catalyze ATP hydrolysis relative to the aqueous phase, it stands to reason that a more aqueouslike environment will have a higher free energy barrier, which is precisely what we see with the ADP run in Figure 8. It is also important to note the difficulty of comparing our reaction thermodynamics to those measured in solution. While the ADP structure environment is open and aqueouslike, the observed reaction is endothermic, unlike the exothermic reaction in solution. This is undoubtably due to our product state, which contains two charged groups in proximity to each other. The release of the phosphate from the binding pocket should be exothermic, resulting in an overall free energy change more similar to the observed aqueous reaction.

It is important to note that many factors go into the conformational changes in protein catalysis. A definitive answer on the role of conformational changes in the catalysis of hydrolysis would require extensive free energy sampling connecting all the states observed here. Such a study has been recently performed for a coarse-grained model of F_1-ATPase.[84] Based on their decomposition of the energy contributions, our current results provide accurate information on the chemical steps of the process, showing that hydrolysis is preferred in the ATP-bound state. We leave exploration of substrate binding and explicit consideration of the conformational path to future studies.

■ CONCLUSIONS

We have reported the first molecular simulation-based study of ATP hydrolysis in a member of the kinesin superfamily. Through the use of QM/MM metadynamics simulations, we examined a combined 13 possible reaction mechanisms starting from initial configurations generated from two previously solved crystal structures, referred to here as the ATP and ADP structures. The size of the QM region (∼200 atoms) and the cumulative simulation time (∼0.7 ns) represents a major computational undertaking. Our study confirms that the ATP structure is more amenable to ATP hydrolysis than the ADP structure, finding both a lower reaction barrier and more stable products for the former. We have found that the most favorable reaction mechanism involves water acting as the catalytic base, which has been hypothesized and confirmed by previous experimental studies. Through the action of the second water (and, in one run, the involvement of a conserved serine), the proton is shuttled to Glu270 of the switch I/II salt bridge, where it is later transferred back to the HPO_4^{2-} ion. These features have been seen in previous studies of both F_1-ATPase and myosin, suggesting a common mechanism across all molecular motors.

Despite the similarities, however, we also found the reaction occurred in a configuration with a broken switch I−switch II salt bridge, which is not the catalytic structure previously suggested. Previous studies on myosin have either limited themselves to exploring a mostly associative mechanism,[9,83] found an associative mechanism,[8] or found a very flat energy landscape for which all different mechanisms are similar in energy,[82] while our results indicate a concerted (or, at least, a nonassociative) mechanism. Recent experimental results on this system have also hypothesized an associative mechanism.[29] In addition, our free energy estimate of 11 ± 3 kcal/mol for the reaction barrier is below the experimental estimate of 17.5 kcal/mol. This is probably due to known issues in using density functionals without exact exchange to describe energetics of the reaction. Future studies should focus on using more general collective variables, more exact density functionals, longer simulation times, and multiple runs for the same collection variable starting from different configurations to converge the free energy estimates, although the conditions reported here already push the boundaries of current computational capacities.

■ ASSOCIATED CONTENT

Ⓢ Supporting Information

Additional text, 15 figures, and two tables on collective variables and metadynamics as described in the text; animations of the reaction processes of ATP.5 (si_002.avi) and ADP.3

(si_003.avi). This material is available free of charge via the Internet at http://pubs.acs.org.

AUTHOR INFORMATION

Corresponding Author

mcgrath@theory.biophys.kyoto-u.ac.jp; takada@biophys.kyoto-u.ac.jp

Notes

The authors declare no competing financial interest.

ACKNOWLEDGMENTS

Xmgrace, VMD, Inkscape, R, and GIMP were used in preparation of the figures. NAMD was developed by the Theoretical and Computational Biophysics Group in the Beckman Institute for Advanced Science and Technology at the University of Illinois at Urbana−Champaign. The study was supported by Grant-in-Aid for Scientific Research on Innovative Areas to S.T. (23107716) and to S.H. (23107717) from the Ministry of Education, Culture, Sports, Science, and Technology, Japan; by Grant-in-Aid for Scientific Research to S.T. (23370057) and to S.H. (23700580); by the Programme for Promotion of Basic and Applied Researches for Innovations in Bio-oriented Industry to S.H.; and by Research and Development of the Next-Generation Integrated Simulation of Living Matter to S.T. and S.H. Part of this research was performed under the auspices of the U.S. Department of Energy by Lawrence Livermore National Laboratory. We thank Liam Krauss (LLNL) for help with the table of contents graphic.

REFERENCES

(1) Hirokawa, N.; Noda, Y.; Tanaka, Y.; Niwa, S. *Nat. Rev. Mol. Cell Biol.* **2009**, *10*, 682−696.

(2) Svoboda, K.; Schmidt, C. F.; Schnapp, B. J.; Block, S. M. *Nature* **1993**, *365*, 721−727.

(3) Yildiz, A.; Tomishige, M.; Vale, R. D.; Selvin, P. R. *Science* **2004**, *303*, 676−678.

(4) Kikkawa, M.; Sablin, E. P.; Okada, Y.; Yajima, H.; Fletterick, R. J.; Hirokawa, N. *Nature* **2001**, *411*, 439−445.

(5) Woehlke, G.; Ruby, A. K.; Hart, C. L.; Ly, B.; Hom-Booher, N.; Vale, R. D. *Cell* **1997**, *90*, 207−216.

(6) Åqvist, J.; Kolmodin, K.; Florián, J.; Warshel, A. *Curr. Biol.* **1999**, *6*, R71−R80.

(7) Schweins, T.; Langen, R.; Warshel, A. *Nat. Struct. Biol.* **1994**, *1*, 476−484.

(8) Schwarzl, S. M.; Smith, J. C.; Fischer, S. *Biochemistry* **2006**, *45*, 5830−5847.

(9) Li, G.; Cui, Q. *J. Phys. Chem. B* **2004**, *108*, 3342−3357.

(10) Grigorenko, B. L.; Nemukhin, A. V.; Shadrina, M. S.; Topol, I. A.; Burt, S. K. *Proteins: Struct., Funct., Bioinf.* **2007**, *66*, 456−466.

(11) Dittrich, M.; Hayashi, S.; Schulten, K. *Biophys. J.* **2003**, *85*, 2253−2266.

(12) Dittrich, M.; Hayashi, S.; Schulten, K. *Biophys. J.* **2004**, *87*, 2954−2967.

(13) Hayashi, S.; Ueno, H.; Shaikh, A. R.; Umemura, M.; Kamiya, M.; Ito, Y.; Ikeguchi, M.; Komoriya, Y.; Iino, R.; Noji, H. *J. Am. Chem. Soc.* **2012**, *134*, 8447−8454.

(14) Grigorenko, B. L.; Rogov, A. V.; Topol, I. A.; Burt, S. K.; Martinez, H. M.; Nemukhin, A. V. *Proc. Natl. Acad. Sci. U.S.A.* **2007**, *104*, 7057−7061.

(15) Grigorenko, B. L.; Kaliman, I. A.; Nemukhin, A. V. *J. Mol. Graphics Modell.* **2011**, *31*, 1−4.

(16) Prasad, B. R.; Plotnikov, N. V.; Warshel, A. *J. Phys. Chem. B* **2013**, *117*, 153−163.

(17) Onishi, H.; Mochizuki, N.; Morales, M. F. *Biochemistry* **2004**, *43*, 3757−3763.

(18) Beke-Somfai, T.; Lincoln, P.; Nordén, B. *Proc. Natl. Acad. Sci. U.S.A.* **2011**, *108*, 4828−4833.

(19) Schlichting, I.; Berendzen, J.; Chu, K.; Stock, A. M.; Maves, S. A.; Benson, D. E.; Sweet, R. M.; Ringe, D.; Petsko, G. A.; Sligar, S. G. *Science* **2000**, *287*, 1615−1622.

(20) Isaev, A.; Scheiner, S. *J. Phys. Chem. B* **2001**, *105*, 6420−6426.

(21) Fisher, Z.; Prada, J. A. H.; Tu, C.; Duda, D.; Yoshioka, C.; An, H.; Govindasamy, L.; Silverman, D. N.; McKenna, R. *Biochemistry* **2005**, *44*, 1097−1105.

(22) Takahashi, H.; Hashimoto, H.; Nitta, T. *J. Chem. Phys.* **2003**, *119*, 7964−7971.

(23) Loerting, T.; Liedl, K. R. *J. Phys. Chem. A* **2001**, *105*, 5137−5145.

(24) Olsson, M. H. M.; Warshel, A. *Proc. Natl. Acad. Sci. U.S.A.* **2006**, *103*, 6500−6505.

(25) Braun-Sand, S.; Burykin, A.; Chu, Z. T.; Warshel, A. *J. Phys. Chem. B* **2005**, *109*, 583−592 (PMID 1685105).

(26) Braun-Sand, S.; Strajbl, M.; Warshel, A. *Biophys. J.* **2004**, *87*, 2221−2239.

(27) Kato, M.; Pisliakov, A. V.; Warshel, A. *Proteins: Struct., Funct., Bioinf.* **2006**, *64*, 829−844.

(28) Parke, C. L.; Wojcik, E. J.; Kim, S.; Worthylake, D. K. *J. Biol. Chem.* **2010**, *285*, 5859−5867.

(29) Jun, B.; Kim, S. *J. Biol. Chem.* **2010**, *285*, 11073−11077.

(30) Valentine, M. T.; Gilbert, S. P. *Curr. Opin. Cell Biol.* **2007**, *19*, 75−81.

(31) Kashina, A. S.; Rogers, G. C.; Scholey, J. M. *Biochim. Biophys. Acta* **1997**, *1357*, 257−271.

(32) Peterman, E. J. G.; Scholey, J. M. *Curr. Biol.* **2009**, *19*, R1089−R1094.

(33) Endow, S. A.; Kull, F. J.; Liu, H. *J. Cell Sci.* **2010**, *123*, 3420−3424.

(34) Tanenbaum, M. E.; Medema, R. H. *Dev. Cell* **2010**, *19*, 797−806.

(35) Krzysiak, T. C.; Grabe, M.; Gilbert, S. P. *J. Biol. Chem.* **2008**, *283*, 2078−2087.

(36) Turner, J.; Anderson, R.; Guo, J.; Beraud, C.; Fletterick, R.; Sakowicz, R. *J. Biol. Chem.* **2001**, *276*, 25496−25502.

(37) Kull, F. J.; Endow, S. A. *J. Cell Sci.* **2002**, *115*, 15−23.

(38) Lin, H.; Truhlar, D. *Theor. Chem. Acc.* **2007**, *117*, 185−199.

(39) Kamerlin, S. C. L.; Haranczyk, M.; Warshel, A. *J. Phys. Chem. B* **2009**, *113*, 1253−1272.

(40) Laio, A.; Parrinello, M. *Proc. Natl. Acad. Sci. U.S.A.* **2002**, *99*, 12562−12566.

(41) Boero, M.; Ikeda, T.; Ito, E.; Terakura, K. *J. Am. Chem. Soc.* **2006**, *128*, 16798−16807.

(42) Glaves, R.; Mathias, G.; Marx, D. *J. Am. Chem. Soc.* **2012**, *134*, 6995−7000.

(43) Eswar, N.; Marti-Renom, M. A.; Webb, B.; Madhusudhan, M. S.; Eramian, D.; Shen, M.; Pieper, U.; Sali, A. *Current Protocols in Bioinformatics, Supplement 15*; John Wiley & Sons: New York, 2006.

(44) Humphrey, W.; Dalke, A.; Schulten, K. *J. Mol. Graphics* **1996**, *14*, 33−38.

(45) Pavelites, J. J.; Gao, J.; Bash, P. A.; MacKerell, A. D., Jr. *J. Comput. Chem.* **1997**, *18*, 221−239.

(46) MacKerell, A. D., Jr.; et al. *J. Phys. Chem. B* **1998**, *102*, 3586−3616.

(47) Jorgensen, W. L.; Chandrasekhar, J.; Madura, J. D.; Impey, R. W.; Klein, M. L. *J. Chem. Phys.* **1983**, *79*, 926−935.

(48) Pecoraro, V. L.; Hermes, J. D.; Cleland, W. W. *Biochemistry* **1984**, *23*, 5262−5271.

(49) Hess, B.; Kutzner, C.; van der Spoel, D.; Lindahl, E. *J. Chem. Theory Comput.* **2008**, *4*, 435−447.

(50) Miyamoto, S.; Kollman, P. A. *J. Comput. Chem.* **1992**, *13*, 952−962.

(51) Hess, B. *J. Chem. Theory Comput.* **2008**, *4*, 116−122.

(52) Berendsen, H. J. C.; Postma, J. P. M.; van Gunsteren, W. F.; DiNola, A.; Haak, J. R. *J. Chem. Phys.* **1984**, *81*, 3684−3690.
(53) Essmann, U.; Perera, L.; Berkowitz, M. L.; Darden, T.; Lee, H.; Pedersen, L. G. *J. Chem. Phys.* **1995**, *103*, 8577−8593.
(54) Laino, T.; Mohamed, F.; Laio, A.; Parrinello, M. *J. Chem. Theory Comput.* **2005**, *1*, 1176−1184.
(55) Hu, L.; Söderhjelm, P.; Ryde, U. *J. Chem. Theory Comput.* **2011**, *7*, 761−777.
(56) CP2K Developers, *Open Source Molecular Dynamics*. http://www.cp2k.org
(57) Kohn, W.; Sham, L. J. *Phys. Rev.* **1965**, *140*, A1133−A1138.
(58) VandeVondele, J.; Krack, M.; Mohamed, F.; Parrinello, M.; Chassaing, T.; Hutter, J. *Comput. Phys. Commun.* **2005**, *167*, 103−128.
(59) Becke, A. D. *Phys. Rev. A* **1988**, *38*, 3098−3100.
(60) Lee, C.; Yang, W.; Parr, R. G. *Phys. Rev. B* **1988**, *37*, 785−789.
(61) Grimme, S.; Antony, J.; Ehrlich, S.; Krieg, H. *J. Chem. Phys.* **2010**, *132*, No. 154104.
(62) Antony, J.; Grimme, S. *Phys. Chem. Chem. Phys.* **2006**, *8*, 5287−5293.
(63) Harrison, C. B.; Schulten, K. *J. Chem. Theory Comput.* **2012**, *8*, 2328−2335.
(64) Klähn, M.; Braun-Sand, S.; Rosta, E.; Warshel, A. *J. Phys. Chem. B* **2005**, *109*, 15645−15650.
(65) Ensing, B.; de Vivo, M.; Liu, Z.; Moore, P.; Klein, M. L. *Acc. Chem. Res.* **2006**, *39*, 73−81.
(66) Laio, A.; Gervasio, F. L. *Rep. Prog. Phys.* **2008**, *71*, No. 126601.
(67) Singh, S.; Chopra, M.; de Pablo, J. J. *Annu. Rev. Chem. Biomol. Eng.* **2012**, *3*, 369−394.
(68) Bussi, G.; Laio, A.; Parrinello, M. *Phys. Rev. Lett.* **2006**, *96*, No. 090601.
(69) Kamerlin, S. C. L.; Warshel, A. *Comput. Mol. Sci.* **2011**, *1*, 30−45.
(70) Štajbl, M.; Shurki, A.; Warshel, A. *Proc. Natl. Acad. Sci. U.S.A.* **2003**, *100*, 14834−14839.
(71) Plotnikov, N. V.; Kamerlin, S. C. L.; Warshel, A. *J. Phys. Chem. B* **2011**, *115*, 7950−7962.
(72) Ensing, B.; Klein, M. L. *Proc. Natl. Acad. Sci. U.S.A.* **2005**, *102*, 6755−6759.
(73) Laio, A.; Rodriguez-Fortea, A.; Gervasio, F. L.; Ceccarelli, M.; Parrinello, M. *J. Phys. Chem. B* **2005**, *109*, 6714−6721.
(74) Raiteri, P.; Laio, A.; Gervasio, F. L.; Micheletti, C.; Parrinello, M. *J. Phys. Chem. B* **2006**, *110*, 3533−3539.
(75) Bonomi, M.; Barducci, A.; Parrinello, M. *J. Comput. Chem.* **2009**, *30*, 1615−1621.
(76) Frushicheva, M. P.; Cao, J.; Warshel, A. *Biochemistry* **2011**, *50*, 3849−3858.
(77) Cochran, J. C.; Gilbert, S. P. *Biochemistry* **2005**, *44*, 16633−16648.
(78) Cochran, J. C.; Krzysiak, T. C.; Gilbert, S. P. *Biochemistry* **2006**, *45*, 12334−12344.
(79) Warshel, A.; Sussman, F.; Hwang, J.-K. *J. Mol. Biol.* **1988**, *201*, 139−159.
(80) Nemukhin, A. V.; Grigorenko, B. L.; Lushchekina, S. V.; Varfolomeev, S. D. *Russ. Chem. Rev.* **2012**, *81*, 1011−1025.
(81) Goyal, P.; Ghosh, N.; Phatak, P.; Clemens, M.; Gaus, M.; Elstner, M.; Cui, Q. *J. Am. Chem. Soc.* **2011**, *133*, 14981−14997.
(82) Yang, Y.; Cui, Q. *J. Phys. Chem. A* **2009**, *113*, 12439−12446.
(83) Yang, Y.; Yu, H.; Cui, Q. *J. Mol. Biol.* **2008**, *381*, 1407−1420.
(84) Mukherjee, S.; Warshel, A. *Proc. Natl. Acad. Sci. U.S.A.* **2011**, *108*, 20550−20555.